

Generalized Space-Time Autoregressive Modeling of the Vertical Distribution of Copper and Gold Grades with a Porphyry-Deposit Case Study

Udjianna S. Pasaribu^a, Utriweni Mukhaiyar^a, Mohamad N. Heriawan^b, Yundari Yundari^{c,*}

^a Statistics Division Faculty of Mathematics and Natural Sciences, Institut Teknologi Bandung, Bandung, Indonesia

^b Earth Resources Exploration Research Group, Faculty of Mining and Petroleum Engineering, Institut Teknologi Bandung, Bandung, Indonesia

^c Mathematics Department, Faculty of Mathematics and Natural Sciences, Universitas Tanjungpura, Pontianak, Indonesia

Corresponding author: *yundari@math.untan.ac.id

Abstract—We examined the first-order application of the generalized space-time autoregressive GSTAR (1;1) model. The autoregressive model was used and was performed simultaneously in multiple drill-hole locations. The GSTAR model was applied to data with absolute time parameter units, such as hours, days, months, or years. Here a new perspective on modeling space-time data is raised. We used the relative time parameter index as a discretization of the same drilling depth of mineralization through a porphyritic deposit. Random variables were the copper and gold grades derived from the hydrothermal fluid that passed through the rock fractures in a porphyry copper deposit in Indonesia. This research aims to model the vertical distribution of copper and gold grades through backcasting the GSTAR (1;1) model. Such results could help geologists to predict copper and gold grades in deeper zones in an ore deposit. Two spatial weight matrices were used in the GSTAR (1;1) model, and these were based on a Euclidean distance and kernel function. Both weight matrices were constructed from different perspectives. The Euclidean distance approach gave a fixed weight matrix. Meanwhile, the kernel function approach gave the possibility to be random since it is based on real observations. It is obtained that the estimated (in-sample) and predicted (out-sample) kernel weight approach was accurate. Copper and gold grades data could recommend the GSTAR (1;1) model with a spatial kernel weight for modeling the vertical continuity case.

Keywords— Space-time model; back-casting; autoregressive; hydrothermal fluid.

*Manuscript received 1 Apr. 2021; revised 9 Sep. 2021; accepted 15 Oct. 2021. Date of publication 31 Oct. 2022.
IJASEIT is licensed under a Creative Commons Attribution-Share Alike 4.0 International License.*



I. INTRODUCTION

Hydrothermal alterations are mineralogical changes and compositions in rocks interacting with hydrothermal fluids. A hydrothermal fluid is a hot liquid derived from the earth's crust and moves upward with the components of the ore mineral. Hydrothermal fluids can be derived from magmatic, meteoric, or mineral-connated liquid that is produced during metamorphism and becomes hot inside the earth [1], [2]. Hydrothermal alteration is closely associated with mineralization because a typical primary mineralization will characterize a certain type of alteration. Mineralization is the process of forming minerals in the body of the rock and is caused by a magmatic process. Hydrothermal alteration is one of the processes that can cause mineralization. Hydrothermal fluid interacts with rock past which it moves, and carries

anions or cations from these rocks, which can bind mineral-forming compounds. During cooling, the fluids become saturated and later form mineral deposits that can bear ore or metal-containing minerals, such as copper, gold, silver, and molybdenum [3]. This mineralization process also relies on porphyry precipitation [4], [5]. Geological modeling aims to interpolate unobserved locations to locate exploration targets. For example, a porphyry exploration target deposit is based on metallic zonation [4]–[6]. Modeling is used to predict particular locations (laterally) and to predict subsurface (vertical) composition. In fact, a prediction of the mineralogy in deeper zones is important to locate exploration targets and determine the possibility of significant metal grades in these zones.

The formation of subsurface mineral deposits meets the superposition principle of mineralization where the lower zone is older than the upper zones because the hydrothermal

fluid moves upwards. In the presence of hydrothermal alteration, a measure (data) can be obtained, one of which is the copper (Cu) and gold (Au) grades as determined from an analysis of the drill-core sample. By considering the depth as an index of time parameters and the number of drilling locations as an index of location parameters, the Cu (in %) and Au (in ppm) grades can be modeled in a stochastic process. A stochastic process of state space with an index of time and location parameters was analyzed by space-time analysis. The well-known linear space-time model was the space-time autoregressive (STARMA) model [7], [8]. One such model is the STAR model, which has the same autoregressive (AR) parameter for each location. A generalized model was developed to accommodate diversity among locations and was termed the generalized space-time autoregressive (GSTAR) model [9].

Suppose a stochastic process $\{Y_i(t)\}$ exists that represents an observation at location- i , where $i = 1, 2, \dots, N$, and at time- t , where $t = 1, 2, \dots, T$. N represents the number of locations (spatial) and T represents the number of observations with time. This process follows the GSTAR($p; \lambda_1, \lambda_2, \dots, \lambda_p$) model. It represents the autoregressive terms lagged in the p -th order in time and the order of $(\lambda_1, \lambda_2, \dots, \lambda_p)$ in space. If the column vector $\mathbf{Y}(t) = (Y_1(t), Y_2(t), \dots, Y_N(t))'$ can be presented as:

$$\mathbf{Y}(t) = \Phi_1 \mathbf{Y}(t-1) + \Phi_2 \mathbf{Y}(t-2) + \dots + \Phi_p \mathbf{Y}(t-p) + \boldsymbol{\varepsilon}(t) \quad (1)$$

where $\Phi_1, \Phi_2, \dots, \Phi_p$ are parameter matrices that define

$$\Phi_k = \Phi_{k0} + \sum_{\ell=0}^{\lambda_p} \Phi_{k\ell} \mathbf{W}^{(\ell)}$$

and $\boldsymbol{\varepsilon}(t) = (\varepsilon_1(t), \varepsilon_2(t), \dots, \varepsilon_N(t))'$.

The matrices $\Phi_{k\ell}$ and $\mathbf{W}^{(\ell)}$ define the autoregressive parameter matrix in the time lag k , spatial lag ℓ and the weight matrix on the spatial lag ℓ . The simplest GSTAR model class is GSTAR (1;1), which assumes a time order $p = 1$ and a spatial order $\lambda_1 = 1$. Based on Eq. (1), the model GSTAR (1;1) was formulated as:

$$\mathbf{Y}(t) = \Phi_1 \mathbf{Y}(t-1) + \boldsymbol{\varepsilon}(t) \quad (2)$$

in which $\Phi_1 = \Phi_{10} + \Phi_{11} \mathbf{W}$ and $\mathbf{W}^{(1)} = \mathbf{W}$. We used the GSTAR (1;1) model to model the case study because it is based on a close location and time interval, i.e., 2 meters, therefore, this model can still represent the data.

The GSTAR model applications have been used in varied applications, such as to model tea plantation production [9], [10]), the Gamma ray log [11], the Covid-19 data [12], [13], and the coffee borer beetle attacks[14]. This research used GSTAR to model the space-time data of the Cu and Au grades. Because hydrothermal fluid flowed from the deeper zone upward through the wallrocks, the time parameter was the depth of mineralization. The deeper mineralization became the starting time (elder), and the younger time [1] was that moving upward through the upper mineralization. This application is novel in space-time modeling research, especially when using the GSTAR model. This method used to model the vertical continuity of Cu and Au grades in a porphyry deposit in Indonesia and would enable geologists to predict Cu and Au grades in unknown deeper deposit zones.

II. MATERIALS AND METHODS

This section explains the comprehensive theoretical basis. The first subsection explains the general geology of porphyritic copper deposits. The second subsection introduces the generalized space-time autoregressive model.

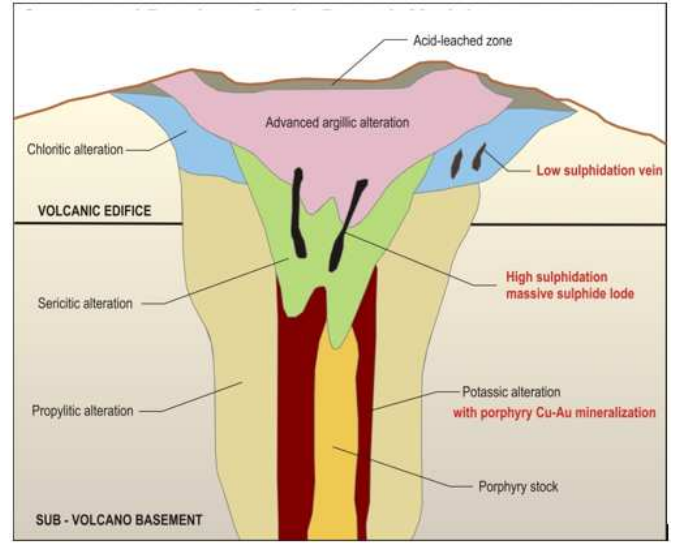


Fig. 1 Conceptual model of hydrothermal deposit system [15]

A. Porphyritic copper deposit

The porphyry deposit was derived originally from an acid-intermediate intrusion, which occurs in contact with the wall rocks that produce mineralization. The main porphyry deposit product was a Cu-Au or Cu-Mo mineralization. Porphyry deposits were formed from several intrusion activities consisting of a collection of dike and intrusion breccia. The mineralization that resulted from alteration occurred as disseminated and stockwork ores. The alteration occurred intensively and extensively through the hostrock from hydrothermal fluids. Mining methods for such deposits commonly include open pit mines because the porphyry copper deposits tend to be large. Low to medium copper grades tend to be <1% Cu, whereas if the copper is combined with other elements, the Cu levels range from 0.6% to 0.9%[15].

Fig. 1 provides a conceptual model of a hydrothermal deposit system in which the presence of a porphyritic deposit is associated with a low sulphidation vein and a high sulphidation massive sulphide lode. Spatial and temporal-related relations with subduction may affect the rock characteristics in porphyry copper deposits. Therefore, subduction played a major role during the formation. This process always occurred in calc-alkaline to alkaline igneous rocks and resulted in a variation in the concentrations of metals. The chemical variations of intrusions showed that the most likely source of metals originated from the igneous rocks [15].

The porphyry deposit used in this study is located in North Sulawesi, Indonesia. According to [16], the geology at study site is dominated by the product of volcanic activity and intrusion. Intrusion rocks at this study site included quartz diorite to diorite that intruded the volcanic rock formation, and the mineralization was associated with intrusion rocks. The hydrothermal alteration was developed strongly with

types of stockwork silica K-silicate (quartz, magnetite, biotite) that were overprinted by moderate argillic (sericite, illite, chlorite), and then replaced by advanced argillic alterations (vuggy silica, alunite, kaolinite, some native sulfur). The local geology of the study site is depicted in Fig. 2.

B. Generalized Space-time AR Model

If we consider a stochastic process $\{Y_i(t)\}$ in which $t = 1, \dots, T, i = 1, \dots, N, T$ represents the number of observations in time and N represents the number of locations (spatial). The first order of GSTAR (1;1) model is given by [10]:

$$Y_i(t) = \phi_{0i}Y_i(t-1) + \phi_{1i} \sum_{j=1}^N W_{ij}Y_j(t-1) + \varepsilon_i(t) \quad (3)$$

where $Y_i(t)$ is the observation at time t in location i , ϕ_{0i} and ϕ_{1i} represent autoregressive parameters for time and location, respectively, W_{ij} is the spatial weight, and $\varepsilon_i(t)$ is the model error at time t in location i . As an illustration, assume that $Y_i(t)$ represents the Cu grades in drill-hole- i at a relative time- t . The relative time t was obtained by discretizing the depth with the same intervals. Therefore, the Cu grade in the deepest zone will be the first observation in drill-hole- i , termed $Y_i(1)$, and the Cu grade in the top zone (nearest the plant view) will be the last observation in drill-hole- i , termed $Y_i(T)$. If $Y_i(t)$ Following the GSTAR (1;1) model, the Cu grades in drill-hole- i at a relative time- t will be influenced by the Cu grades in the previous (lower) zone of the same drill-hole and the nearest-neighbor drill-holes.

The spatial weight matrix with element W_{ij} is nonzero at a measurement of different locations $i \neq j$. The uniform weight is defined as $W_{ij} = \frac{1}{n_i}$, in which n_i denotes the number of locations i . This weight gives the same values for all elements in the same row, except for the main diagonal, and these values are influenced by the number of locations within an observed spatial lag. The binary weight has a value of 0 and 1

in each row, except for the main diagonal, which is 0. The value 1 represents that location j that gives the greatest weight (dominant) to location i . The spatial weights as based on Euclidean distances (d_{ij}) is defined as $W_{ij} = \frac{d_{ij}}{\sum_{k=1}^N d_{ik}}$.

The three spatial weights are given (fixed) and subjective. We introduced a new method to construct the spatial weight matrix. This method uses observed data that becomes the domain of the kernel function. Usually, the kernel functions were used to estimate the probability density function and regression function. Research on the kernel has been investigated ([17]–[20]). In this paper, we propose a new approach to determine the spatial weight matrix of the GSTAR (1;1) model by using a kernel function ([20], [21]). The obtained spatial weights may be random (they depend on an observed value) and are no longer subjective in this research. By using the mean value of each location \bar{Y}_i , the location weights j to i can be written as:

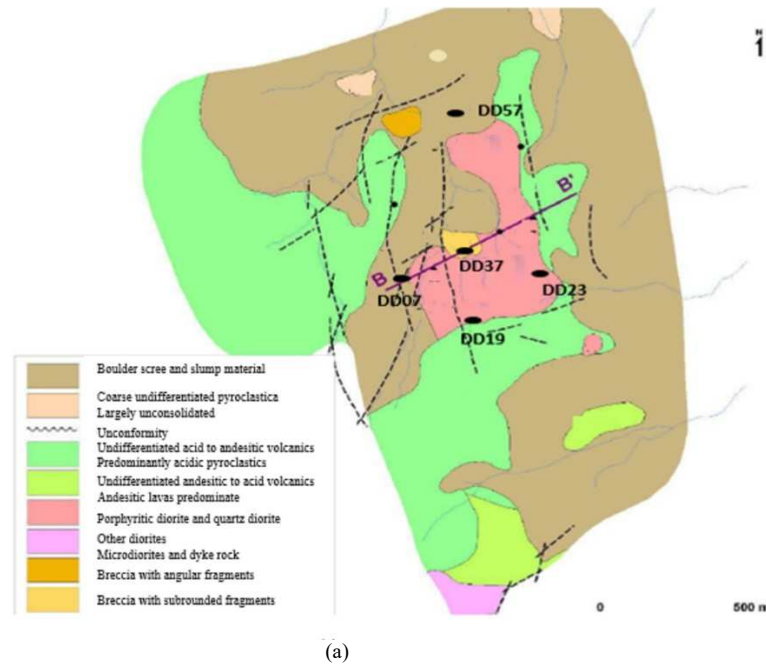
$$W_{ij} = \frac{k\left(\frac{\bar{Y}_i - \bar{Y}_j}{h}\right)}{\sum_{\substack{l=1 \\ l \neq i}}^N k\left(\frac{\bar{Y}_i - \bar{Y}_l}{h}\right)} \quad (4)$$

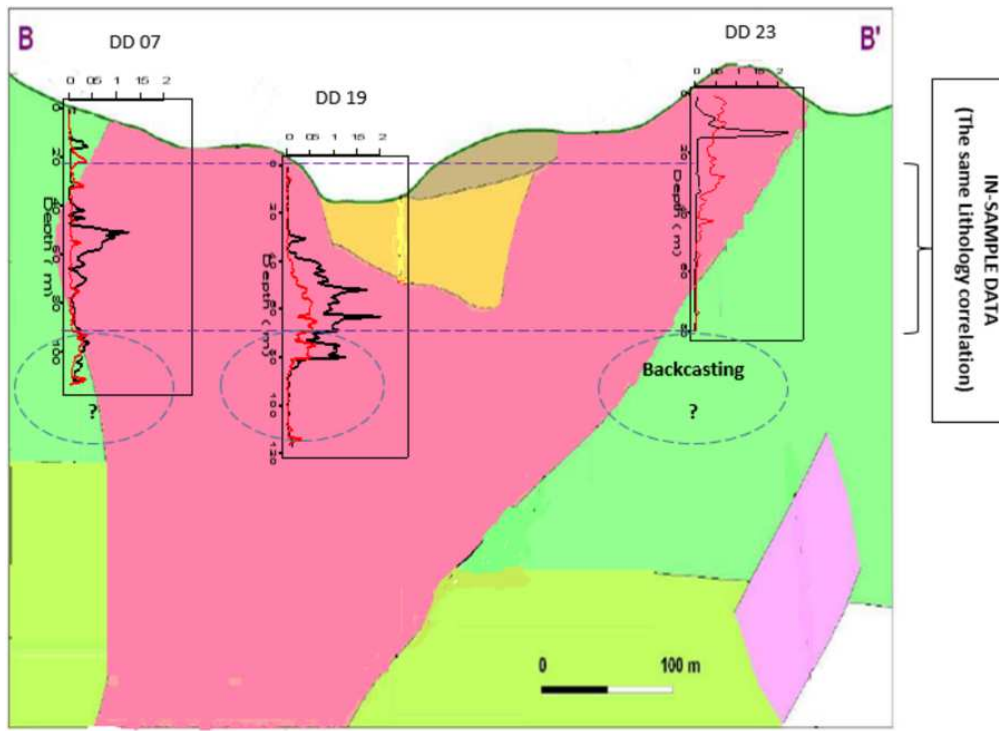
where h is the bandwidth that controls the smoothness level and k is the kernel function.

The parameter of estimation of GSTAR (1;1) will be modeled by the least-squares method. The following equation represents the linear regression of the GSTAR (1;1) model. For $t = 1, 2, \dots, T$, a GSTAR (1;1) model can be expressed simultaneously as the following linear model:

$$\mathbf{Y} = \mathbf{X}\Phi + \boldsymbol{\varepsilon} \quad (5)$$

The response vector $\mathbf{Y} = (Y_1, Y_2, \dots, Y_N)'$ in Eq. (5) with elements $Y_i = (Y_i(1), \dots, Y_i(T))'$ for $i = 1, 2, \dots, N$ has a size of $(NT \times 1)$.





(b)

Fig. 2 The location of five drill-holes that contained Cu (black) and Au (red) grades in (a) plan view and (b) cross-section of DD07, DD19, and DD23. The location coordinates of this study were close together, therefore a first order of spatial lag can be represented, and the GSTAR (1; 1) model was used.

The explanatory matrix $\mathbf{X} = \text{diag}(\mathbf{X}_1, \mathbf{X}_2, \dots, \mathbf{X}_N)$ is a $(NT \times 2N)$ -block diagonal matrix that is defined as:

$$\mathbf{X}_i = \begin{pmatrix} Y_i(0) & \sum_{j \in J_i} W_{ij} Y_j(0) \\ Y_i(1) & \sum_{j \in J_i} W_{ij} Y_j(1) \\ \vdots & \vdots \\ Y_i(T-1) & \sum_{j \in J_i} W_{ij} Y_j(T-1) \end{pmatrix} \quad (6)$$

Parameter $\boldsymbol{\Phi} = (\phi_1, \phi_2, \dots, \phi_N)'$ is a $(2N \times 1)$ -vector with $\phi_i = (\phi_{0i}, \phi_{1i})'$. Furthermore, error vector $\boldsymbol{\varepsilon} = (\varepsilon_1, \varepsilon_2, \dots, \varepsilon_N)'$ is a $(NT \times 1)$ -vector with $\varepsilon_i = (\varepsilon_i(1), \varepsilon_i(2), \dots, \varepsilon_i(T))'$. Therefore, parameter $\boldsymbol{\Phi}$ in Eq. (5) can be estimated through the least-squares method.

The next step was to validate the model by using the inverse of the Auto-covariance Matrices (IAcM) approach and a residual test. This stage was used to show the stationary GSTAR (1; 1) model through IAcM that would look for linkages between the sums of the residual squares and IAcM. Then, each IAcM element was established as an explicit function of the model parameter. The estimation and validation of the procedure were done using the inverse of the IAcM approach which has been discussed extensively by previous studies [9], [20]. The performance of the generalized space-time model with its spatial weights was tested via a normality test, and a root mean squares error (RMSE).

III. RESULTS AND DISCUSSION

We applied the GSTAR (1;1) model to Cu and Au grades from five drill-holes (Fig. 2(a)). By discretizing the depth with the same interval of 2 m, an index of time parameters was established as a function of depth. The same relative time was set for each drill-hole based on the same lithology as shown in Fig. 2(b). For the Cu (as a random variable denoted $Y_i(t)$)

and Au (as a random variable denoted $Z_i(t)$) grades at an unobserved depth for drill-hole DD23 with the support of other drill-holes (i.e., DD07 and DD19).

Geologists use common modeling to interpolate unobserved locations. For example, in Fig. 2(a), the metal grade was predicted between DD37 and DD23. In this modeling, we introduced a new breakthrough with the concept of a time series and location dependence to predict the unexamined borehole that is based on Cu and Au grade data (i.e., $Y_i(t)$ and $Z_i(t)$) (Fig. 2 (b)). The possibility of unexamined metal grades in the deeper drill-holes is essential to exploring the substantial potential of the mineral deposit. By assuming the existence of location dependence, each depth from the lower to the upper zones is considered as a relative time, and therefore, space-time modeling for back-casting purposes can be conducted.

The data set consisted of Cu and Au grades with a depth cut off up to 50 m for each drill-hole (location) is described in Fig. 2. This dataset contained 53 observations for five locations (Fig. 3). For back-casting extrapolation purposes, the data were grouped into in- and out-sample data. In-sample data were the first 50 observations used for model development, and out-sample data were the last three data used to compare the back-casting performance. The initial GSTAR (1;1) step was to inspect the stationary data visually and the data mean and variance were not stationary. Therefore, a transformation through differentiation was essential (Fig. 3). This differentiation was carried out by reducing the current observation with the previous observation ($Y_i(t) - Y_i(t-1)$). From the differentiation, the mean became constant, but the variance did not. Because the variance did not occur constantly during a very short time, we assumed that the data were stationary against the mean and variance.

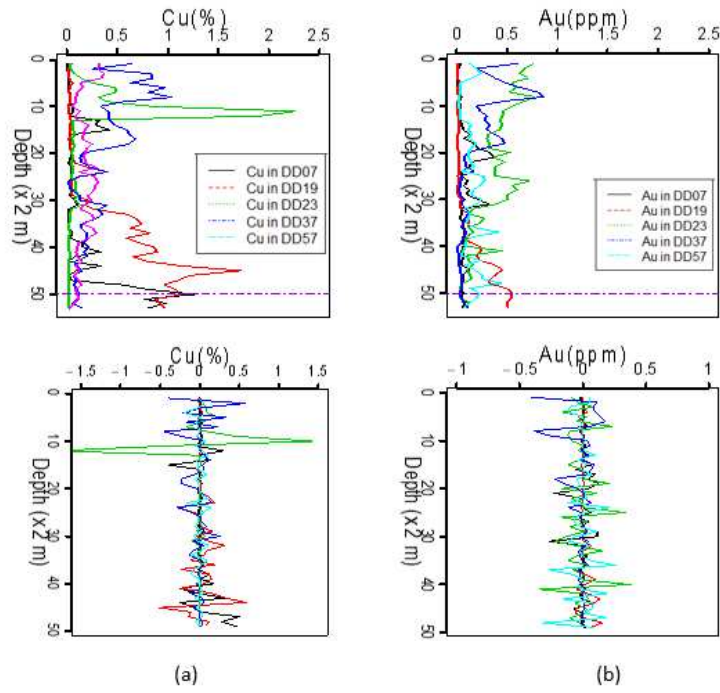


Fig. 3 (a) Plot of Cu grades and their differences, and (b) plot of Au grades and their differences. The data appear to be stationary against the mean and thus were assumed to be stationary for the variance.

TABLE I
LEAST-SQUARES ESTIMATORS AND SIGNIFICANCE TEST FOR THE GSTAR(1;1) PARAMETERS.

Data	Type of spatial weight	Estimation of AR parameters in time term			Estimation of AR parameters in spatial term		
		$\hat{\phi}_{i0}$	$ T_c $	CI 95%	$\hat{\phi}_{i1}$	$ T_c $	CI 95%
Cu	Based distance weight	0.012	33.45	[-0.046, 0.070]	-0.020	30.03	[-0.086, 0.047]
		-0.012	41.76	[-0.060, 0.035]	0.026	20.88	[-0.065, 0.118]
		0.027	85.79	[0.005, 0.049]	-0.063	17.92	[-0.179, 0.053]
		-0.050	45.49	[-0.096, -0.005]	0.006	25.64	[-0.070, 0.082]
		-0.058	18.71	[-0.169, 0.053]	-0.033	29.42	[-0.103, 0.035]
	Gaussian Kernel weight	0.015	51.95	[-0.022, 0.052]	-0.025	55.68	[-0.061, 0.011]
		-0.013	63.84	[-0.044, 0.018]	0.082	36.59	[0.0097, 0.0014]
		0.028	131.56	[0.033, 0.131]	-0.150	34.47	[-0.214, -0.083]
		-0.050	69.74	[-0.079, -0.020]	-0.004	61.32	[-0.036, -0.028]
		-0.055	28.43	[-0.130, 0.018]	-0.020	72.18	[-0.048, 0.008]
Au	Based distance weight	-0.019	50.91	[-0.058, 0.020]	0.018	40.21	[-0.030, 0.066]
		0.021	32.46	[-0.038, 0.080]	-0.015	44.95	[-0.060, 0.029]
		-0.039	99.40	[-0.060, -0.019]	0.059	32.11	[-0.002, 0.117]
		0.020	81.99	[-0.003, 0.044]	-0.039	39.21	[-0.091, 0.013]
		-0.035	80.62	[-0.095, 0.014]	-0.040	37.39	[-0.095, 0.014]
	Gaussian Kernel weight	-0.017	93.88	[-0.038, 0.0044]	-0.0034	78.74	[-0.022, 0.028]
		0.021	59.75	[-0.011, 0.053]	-0.0088	94.02	[-0.030, 0.012]
		-0.037	184.05	[-0.048, -0.026]	0.017	115.14	[0.00007, 0.034]
		0.021	150.92	[0.008, 0.034]	-0.030	120.36	[-0.046, -0.013]
		-0.034	147.51	[-0.048, -0.020]	-0.042	61.41	[-0.075, -0.008]

After transforming the data, the next step was established as a spatial weighting matrix. In this study, we used the spatial matrix that was based on the distance and Gaussian kernel function. The Gaussian kernel function was defined as:

$$k(x) = \frac{1}{\sqrt{2\pi}} \exp\left(-\frac{x^2}{2}\right) \quad (7)$$

Based on the distance weight, W_{dist} , we used the same spatial matrix for Cu and Au grades, but Gaussian kernel spatial weight differed from the following matrix:

From the spatial weight matrix based on distance, the distance of DD19 to DD57 was closest, whereas the distance of DD07 to DD37 was furthest. This weight matrix was the

same for the Cu and Au grades because each drill-holes produced Cu and Au grades together. The spatial weight matrix through the Gaussian kernel produced different weight matrices for the Cu and Au grades. This occurred because the determination of the kernel weight matrix is based on the data of each observation for Cu and Au. In DD07, the Cu grade was almost similar to the data in DD19, whereas the most dissimilar Cu grade occurred between DD07 and DD37. This condition was similar to the weight matrix through the distance for the last weight. Similar Au data existed in DD23 to DD37, whereas the most dissimilar data occurred between DD19 and DD23 and DD19 and DD37. Consequently, a large significant difference existed for the size of the proximity

between the weight matrix based on distance with the Gaussian kernel.

The next step was estimating the parameters using the least-squares method for the GSTAR(1;1) model [10]. Per the procedure described in the before section, the least-squares estimator for each spatial weight matrix GSTAR (1;1) model was obtained (see Table 1). If we consider a null hypothesis $H_0: \hat{\phi}_{k\ell} = \phi_{k\ell}$, and an alternative hypothesis $H_1: \hat{\phi}_{k\ell} \neq \phi_{k\ell}$, then the statistics test is:

$$T_c = \frac{\hat{\phi}_{k\ell} - \phi_{k\ell}}{\sqrt{\text{Var}(\hat{\phi}_{k\ell})}}$$

which follows the t -distribution and degree of freedom, $v = N(T - 2)$. $\text{Var}(\hat{\phi}_{k\ell})$ represents the corresponding diagonal element of the matrix $s^2(\mathbf{X}'\mathbf{X})^{-1}$. For any level of significance $\alpha < 10\%$, the null hypothesis H_0 was rejected, i.e., $|T_c| > t_{\alpha/2, v}$. The confidence interval, $\phi_{k\ell}$ is defined by:

$\hat{\phi}_{k\ell} - t_{\alpha/2, v} \sqrt{\widehat{\text{Var}}(\hat{\phi}_{k\ell})} \leq \phi_{k\ell} \leq \hat{\phi}_{k\ell} + t_{\alpha/2, v} \sqrt{\widehat{\text{Var}}(\hat{\phi}_{k\ell})}$ The hypothesis test of the AR estimator significance resulted in large t -statistics for all parameters, which implied very small p -values. In this case, the null hypothesis was rejected. We conclude that all estimated parameters were significant. In addition, the diagnostic test through the eigenvalues of a parameter matrix gave absolute values of less than one, and IACM yielded positive values for all principal sub-determinants. Based on [20], both approaches gave the same conclusion that the data were stationary.

The modeling results for the Cu and Au grades based on the distance weight are as follows, respectively:

$$\hat{\mathbf{Y}}(t) = (\Phi_{i0(Y)}^{dist} + \Phi_{i1(Y)}^{dist} \mathbf{W}_{dist}) \mathbf{Y}(t-1) \text{ and}$$

$$\hat{\mathbf{Z}}(t) = (\Phi_{i0(Z)}^{dist} + \Phi_{i1(Z)}^{dist} \mathbf{W}_{dist}) \mathbf{Z}(t-1)$$

where

$$\Phi_{i0(Y)}^{dist} = \begin{pmatrix} 0.01 & 0 & 0 & 0 & 0 \\ 0 & -0.01 & 0 & 0 & 0 \\ 0 & 0 & 0.03 & 0 & 0 \\ 0 & 0 & 0 & -0.05 & 0 \\ 0 & 0 & 0 & 0 & -0.06 \end{pmatrix}, \Phi_{i1(Y)}^{dist} = \begin{pmatrix} -0.02 & 0 & 0 & 0 & 0 \\ 0 & 0.03 & 0 & 0 & 0 \\ 0 & 0 & -0.06 & 0 & 0 \\ 0 & 0 & 0 & 0.01 & 0 \\ 0 & 0 & 0 & 0 & -0.03 \end{pmatrix},$$

$$\Phi_{i0(Z)}^{dist} = \begin{pmatrix} -0.02 & 0 & 0 & 0 & 0 \\ 0 & 0.02 & 0 & 0 & 0 \\ 0 & 0 & -0.04 & 0 & 0 \\ 0 & 0 & 0 & 0.02 & 0 \\ 0 & 0 & 0 & 0 & -0.04 \end{pmatrix},$$

$$\Phi_{i1(Z)}^{dist} = \begin{pmatrix} 0.02 & 0 & 0 & 0 & 0 \\ 0 & -0.02 & 0 & 0 & 0 \\ 0 & 0 & 0.06 & 0 & 0 \\ 0 & 0 & 0 & -0.04 & 0 \\ 0 & 0 & 0 & 0 & -0.04 \end{pmatrix}, \text{ and}$$

$$\mathbf{W}_{dist} = \begin{pmatrix} 0 & 0.26 & 0.30 & 0.12 & 0.32 \\ 0.19 & 0 & 0.20 & 0.21 & 0.40 \\ 0.25 & 0.23 & 0 & 0.18 & 0.34 \\ 0.13 & 0.33 & 0.25 & 0 & 0.29 \\ 0.21 & 0.36 & 0.26 & 0.17 & 0 \end{pmatrix}.$$

The results for the modeling of Cu and Au grades with a Gaussian kernel weight are as follows, respectively:

$$\hat{\mathbf{Y}}(t) = (\Phi_{i0(Y)}^{gauss} + \Phi_{i1(Y)}^{gauss} \mathbf{W}_{gauss}) \mathbf{Y}(t-1)$$

and

$$\hat{\mathbf{Z}}(t) = (\Phi_{i0(Z)}^{gauss} + \Phi_{i1(Z)}^{gauss} \mathbf{W}_{gauss}) \mathbf{Z}(t-1)$$

where

$$\Phi_{i0(Y)}^{gauss} = \begin{pmatrix} 0.02 & 0 & 0 & 0 & 0 \\ 0 & -0.01 & 0 & 0 & 0 \\ 0 & 0 & 0.03 & 0 & 0 \\ 0 & 0 & 0 & -0.05 & 0 \\ 0 & 0 & 0 & 0 & -0.06 \end{pmatrix},$$

$$\Phi_{i1(Y)}^{gauss} = \begin{pmatrix} -0.03 & 0 & 0 & 0 & 0 \\ 0 & 0.08 & 0 & 0 & 0 \\ 0 & 0 & -0.15 & 0 & 0 \\ 0 & 0 & 0 & 0.01 & 0 \\ 0 & 0 & 0 & 0 & -0.02 \end{pmatrix},$$

$$\Phi_{i0(Z)}^{gauss} = \begin{pmatrix} -0.02 & 0 & 0 & 0 & 0 \\ 0 & 0.02 & 0 & 0 & 0 \\ 0 & 0 & -0.04 & 0 & 0 \\ 0 & 0 & 0 & 0.02 & 0 \\ 0 & 0 & 0 & 0 & -0.04 \end{pmatrix}, \text{ and}$$

$$\mathbf{W}_{gauss} = \begin{pmatrix} 0 & 0.84 & 0.10 & 0.01 & 0.05 \\ 0.74 & 0 & 0.15 & 0.03 & 0.08 \\ 0.06 & 0.10 & 0 & 0.36 & 0.48 \\ 0.01 & 0.02 & 0.44 & 0 & 0.53 \\ 0.03 & 0.05 & 0.48 & 0.44 & 0 \end{pmatrix}.$$

A plot of the estimation model and the original data are given in Fig. 4. Fig. 4 shows the fitting results of the Cu and Au grades as calculated from the GSTAR (1;1) model based on distance and Gaussian kernel weight. The red line represents the results as computed by the GSTAR (1;1) model, and the black line represents the original data. These results show that the pattern in the GSTAR (1;1) model is similar to the original data. Table 2 shows the GSTAR (1;1) model with a kernel spatial weight that has a smaller RMSE than the other spatial weights. As a result, the new kernel spatial weight method was chosen as the best approach. The last step was checking the RMSE and Shapiro -Wilk test of the residual as summarized in Table 3. The errors have an independent and identical normal distribution for the confidence interval 5%.

TABLE II
COMPARISON OF RMSE VALUES OF ESTIMATION RESULTS FOR EACH DRILL-HOLES AND GSTAR (1;1) MODEL.

Data	Method	DD07	DD19	DD23	DD37	DD57
Cu	GSTAR (1;1)	0.2526	0.2718	0.3796	0.3277	0.2588
	distance GSTAR (1;1) kernel	0.1397	0.1760	0.3030	0.2122	0.0913
Au	GSTAR (1;1)	0.1922	0.1720	0.2659	0.2055	0.2246
	distance GSTAR (1;1) kernel	0.0789	0.0354	0.1764	0.0917	0.1439

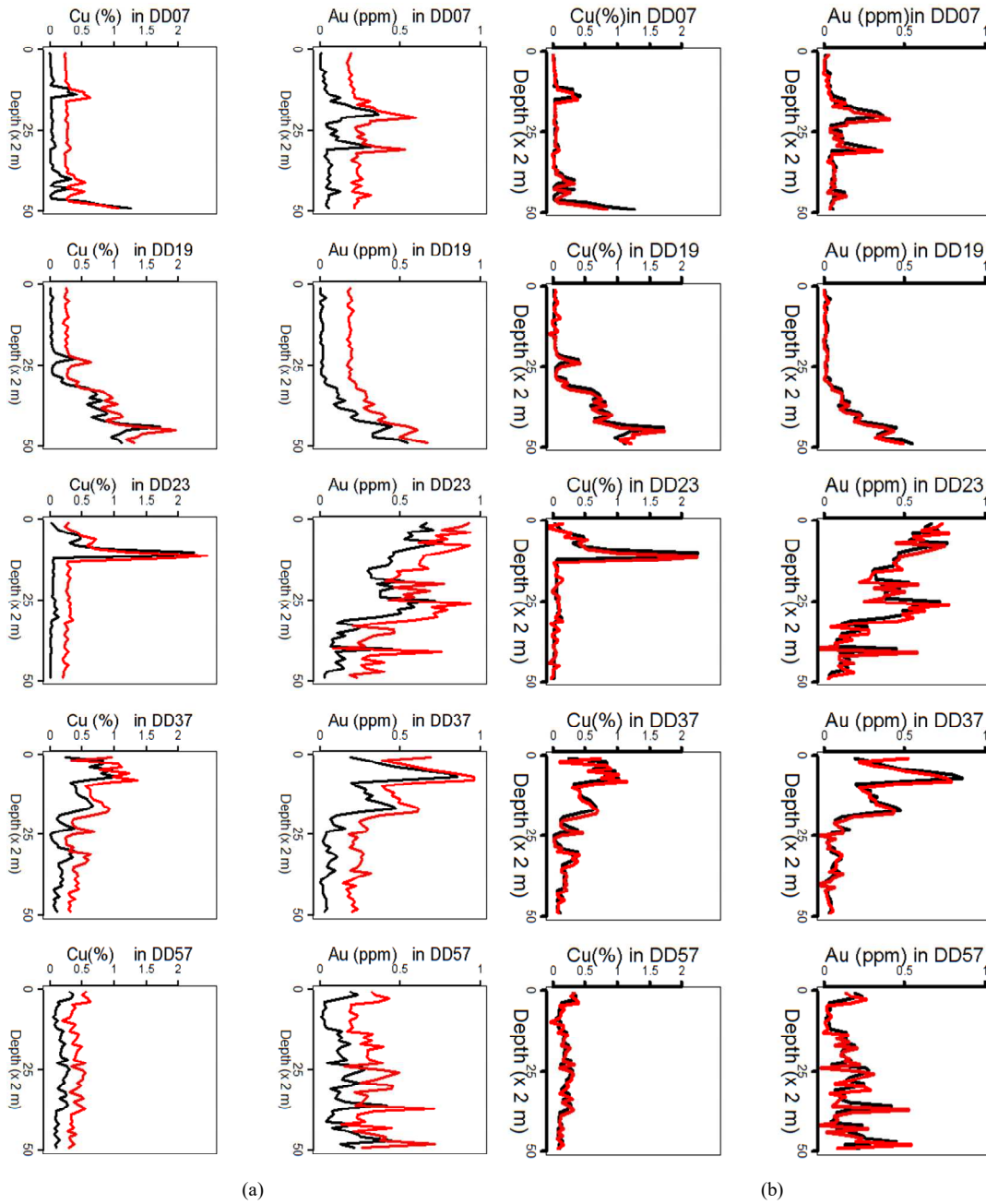


Fig. 4 Original data (black line) and estimations (red line) for each drill-hole. The estimation appears to follow the original data, where (a) modeling is based on the distance spatial weight, and (b) modeling using Gaussian kernel weight.

TABLE III
P-VALUE OF DIAGNOSTIC TEST USING THE SHAPIRO-WILK NORMALITY TEST

Data	Method	DD07	DD19	DD23	DD37	DD57
Cu	GSTAR (1;1) distance	8.161 $\times 10^{-7}$	5.25 x 10^{-4}	3.112 x 10^{-12}	1.78 x 10^{-3}	3.67 x 10^{-1}
	GSTAR (1;1) kernel	1.51 x 10^{-6}	3.64 x 10^{-4}	1.71 x 10^{-11}	2.42 x 10^{-3}	2.91 x 10^{-1}
Au	GSTAR (1;1) distance	1.28 x 10^{-6}	6.65 x 10^{-3}	1.78 x 10^{-3}	1.09 x 10^{-6}	3.56 x 10^{-2}
	GSTAR (1;1) kernel	1.22 x 10^{-6}	2.18 x 10^{-4}	2.09 x 10^{-3}	1.66 x 10^{-6}	3.63 x 10^{-2}

The result from the GSTAR (1;1) modeling with a Gaussian kernel weight matrix was more accurate. The estimated parameter shows a significant result. The curve of estimation results is significantly close to the original value. For back-casting goals, the best estimated model can be used to estimate Cu and Au grades in the lower zone. Because the data were confirmed as a stationary process, m -steps are required to predict the initial Cu and Au grades as defined, respectively, by:

$$\hat{Y}_i(m) = \hat{\Phi}_{10} \hat{Y}_i(m+1) + \hat{\Phi}_{11} W \hat{Y}_i(m+1) \text{ and } \hat{Z}_i(m) = \hat{\Phi}_{10} \hat{Z}_i(m+1) + \hat{\Phi}_{11} W \hat{Z}_i(m+1).$$

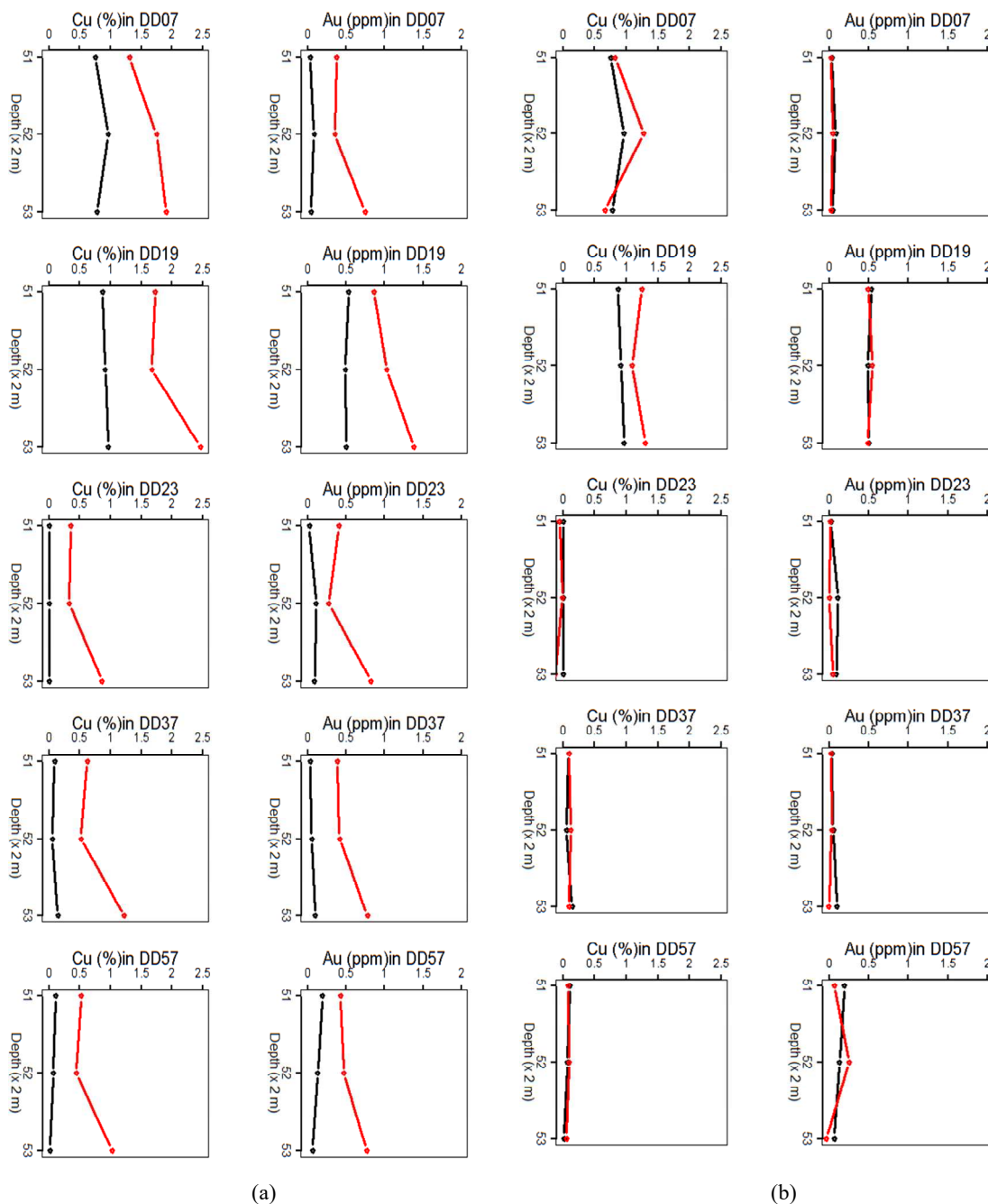


Fig. 5 Comparison of back-casting results of GSTAR (1;1) model (a) based on distance weight, and (b) Gaussian kernel weight. The black curve represents original data and the red curve represents back-casting results.

TABLE IV
COMPARISON OF RMSE VALUES OF PREDICTION RESULTS FOR EACH DRILL-HOLES AND GSTAR (1;1) MODEL.

Data	Method	DD07	DD19	DD23	DD37	DD57
Cu	GSTAR (1;1) distance	1.3564	1.4323	0.9375	1.0456	0.9295
	GSTAR (1;1) kernel	1.1488	0.5120	0.1134	0.0121	0.0240
Au	GSTAR (1;1) distance	0.8081	0.9809	0.8118	0.6922	0.6407
	GSTAR (1;1) kernel	0.0556	0.0029	0.0952	0.0765	0.0627

A comparison of back-casting results by using the three previous observations of the GSTAR (1;1) models is described in Fig. 5. From the back-casting results (out-sample

data), the result for the GSTAR model with a Gaussian kernel weight was very accurate (see Table 4). This corresponds to estimated data (in-sample data) that were improved when using the distance weight matrix. Prediction results indicate that DD07 (West) and DD19 (South) potentially have a Cu grade continuity as the grades exceeded 0.5% Cu. The Au grade also indicated a similar continuity in DD19 (South).

IV. CONCLUSION

The fundamental characteristic of space-time modeling is the spatial weight matrix. We constructed a standard formula to determine the spatial weight matrix that is based on the sample observations data, by using the kernel function as a weight with the mean of the sample observed for each location (the drill-holes) as its domain. To prove the suitability of this new approach, two types of spatial weights

of the GSTAR (1;1) model were compared by using space-time data of Cu and Au grades. The first type was fixed spatial weights, whereas the latter type was a random spatial weight. The kernel weight produced the best results. The kernel weight yielded accurate results in terms of parameter estimation (in-samples) and prediction (out-samples). This result represents a breakthrough in the determination of the spatial weight matrix through the kernel function approach. For Cu and Au grades data, the GSTAR (1;1) model with a spatial kernel weight could be recommended for modeling the vertical continuity. In geosciences, this modeling could be used as a quantitative analysis to predict the vertical continuity of any metal grades in any deposit types.

REFERENCES

- [1] A. Audétat, "The metal content of magmatic-hydrothermal fluids and its relationship to mineralization potential," *Econ. Geol.*, vol. 114, no. 6, pp. 1033–1056, 2019, doi: 10.5382/econgeo.4673.
- [2] Janocko, M. Ryzhkova, T. Mamzina, and S. Bereznev, "Digitalization of economic evaluation of mineral deposits," *E3S Web Conf.*, vol. 105, pp. 1–7, 2019, doi: 10.1051/e3sconf/201910504030.
- [3] A Evans, *Ore Geology and Industrial Minerals an Introduction*. UK: BlackwellScientific, 1993.
- [4] R. H. Sillitoe, "Porphyry copper systems," *Econ. Geol.*, vol. 105, no. 1, pp. 3–41, 2010, doi: 10.2113/gsecongeo.105.1.3.
- [5] M. Yousefi, "Analysis of zoning pattern of geochemical indicators for targeting of porphyry-Cu Mineralization: A Pixel-Based Mapping Approach," *Nat. Resour. Res.*, vol. 26, no. 4, pp. 429–441, 2017.
- [6] F. T. Alain Cheilletz, Ewan Pelleter, Agustin Martin-Izard, "World Skarn Deposits: Skarns of Western Canada," no. Table 8, pp. 1–5, 1996.
- [7] Y. Zhao *et al.*, "A new Seasonal Difference Space-Time Autoregressive Integrated Moving Average (SD-STARIMA) model and spatiotemporal trend prediction analysis for Hemorrhagic Fever with Renal Syndrome (HFRS)," *PLoS One*, vol. 13, no. 11, pp. 1–20, 2018, doi: 10.1371/journal.pone.0207518.
- [8] S. Rathod, B. Gurung, K. N. Singh, and M. Ray, "An improved Space-Time Autoregressive Moving Average (STARMA) model for Modelling and Forecasting of Spatio-Temporal time-series data An improved Space-Time Autoregressive Moving Average (STARMA) model for Modelling and Forecasting of Spatio-Temporal," vol. 72, no. January 2019, 2018.
- [9] U. Mukhaiyar and U. S. Pasaribu, "A new procedure for generalized STAR modeling using IAcM approach," *ITB J. Sci.*, vol. 44 A, no. 2, pp. 179–192, 2012, doi: 10.5614/itbj.sci.2012.44.2.7.
- [10] Yundari, U. S. Pasaribu, and U. Mukhaiyar, "Error assumptions on generalized STAR model," *J. Math. Fundam. Sci.*, vol. 49, no. 2, pp. 136–155, 2017, doi: 10.5614/j.math.fund.sci.2017.49.2.4.
- [11] Yundari, U. S. Pasaribu, U. Mukhaiyar, and M. N. Heriawan, "Spatial Weight Determination of GSTAR(1;1) Model by Using Kernel Function," in *Journal of Physics: Conference Series*, 2018, vol. 1028, no. 1, doi: 10.1088/1742-6596/1028/1/012223.
- [12] M. Amrani and H. Zeghdoudi, "on Multivariate Spatio-Temporal Time Series Models and Causality Test Using Covid-19 Data," *Adv. Math. Sci. J.*, vol. 10, no. 2, pp. 1037–1052, 2020, doi: 10.37418/amsj.10.2.32.
- [13] U. S. Pasaribu, U. Mukhaiyar, N. M. Huda, K. N. Sari, and S. W. Indratno, "Modelling COVID-19 growth cases of provinces in java Island by modified spatial weight matrix GSTAR through railroad passenger's mobility," *Heliyon*, vol. 7, no. 2, p. e06025, 2021, doi: 10.1016/j.heliyon.2021.e06025.
- [14] H. Pramoedyo, A. Ashari, and A. Fadliana, "Forecasting and Mapping Coffee Borer Beetle Attacks Using GSTAR-SUR Kriging and GSTARX-SUR Kriging Models," *ComTech Comput. Math. Eng. Appl.*, vol. 11, no. 2, pp. 65–73, 2020, doi: 10.21512/comtech.v11i2.6389.
- [15] R. Silitoe, "Exploration of Porphyry Copper Lithocaps," *Australas. Inst. Min. Metal. Publ. Ser.*, vol. 9, no. 95, pp. 527–532, 1995.
- [16] T. M. Van Leeuwen and P. E. Pieters, "Mineral deposits of Sulawesi," no. December, 2011, doi: 10.13140/2.1.3843.2322.
- [17] C. H. Fleming and J. M. Calabrese, "A new kernel density estimator for accurate home-range and species-range area estimation," *Methods Ecol. Evol.*, vol. 8, no. 5, pp. 571–579, 2017, doi: 10.1111/2041-210X.12673.
- [18] Y. C. Chen, "A tutorial on kernel density estimation and recent advances," *Biostat. Epidemiol.*, vol. 1, no. 1, pp. 161–187, 2017, doi: 10.1080/24709360.2017.1396742.
- [19] J. Emmanuel Johnson, V. Laparra, A. Pérez-Suay, M. D. Mahecha, and G. Camps-Valls, "Kernel methods and their derivatives: Concept and perspectives for the earth system sciences," *PLoS One*, vol. 15, no. 10 October, pp. 1–30, 2020, doi: 10.1371/journal.pone.0235885.
- [20] K. N. S. Yundari, Nurainul Miftahul Huda, Udjianna S Pasaribu, Utriweni Mukhaiyar, "Stationary Process in GSTAR(1;1) through Kernel Function," 2020.
- [21] S. W. R. Yundari, "Invertibility of Generalized Space-Time Autoregressive Model with Random Weight," *Cauchy J. Mat. Murni dan Apl.*, vol. 6, no. 4, pp. 246–259, 2021.